Anal. Chem. **2009,** *81,* 2317–2324

Molecular Mapping by Low-Energy-Loss Energy-Filtered Transmission Electron Microscopy Imaging

Elisângela M. Linares, Carlos A. P. Leite, Leonardo F. Valadares, Cristiane A. Silva, Camila A. Rezende, and Fernando Galembeck*

Institute of Chemistry, Universidade Estadual de Campinas, Caixa Postal 6154, 13083-970, Campinas, SP, Brazil

Structure−function relationships in supramolecular systems depend on the spatial distribution of molecules, ions, and particles within complex arrays. Imaging the spatial distribution of molecular components within nanostructured solids is the objective of many recent techniques, and a powerful tool is electron spectroscopy imaging in the transmission electron microscope (ESI-TEM) in the low-energy-loss range, 0−80 eV. This technique was applied to particulate and thin film samples of dielectric polymers and inorganic compounds, providing excellent distinction between areas occupied by various macromolecules and particles. Domains differentiated by small changes in molecular composition and minor differences in elemental contents are clearly shown. Slight changes in the molecules produce intensity variations in molecular spectra that are in turn expressed in sets of low-energy-loss images, using the standard energy-filtered transmission electron microscopy (EFTEM) procedures. The molecular map resolution is in the nanometer range and very close to the bright-field resolution achieved for the same sample, in the same instrument. Moreover, contrast is excellent, even though sample exposure to the electron beam is minimal.

Analytical electron microscopy has already made an invaluable contribution to current knowledge on materials properties, and this is growing steadily thanks to the new techniques and procedures that are being developed in many laboratories.[1−4]

Composition mapping is now practiced in different ways and in a large scale. Energy-dispersive X-ray (EDX) elemental maps are currently very common, and they can be acquired even using table-top, low-cost scanning electron microscopes (SEM). Its use is often restricted to elements heavier than Na, but contemporary equipment yields spectral data for lighter elements. Distribution maps showing differences in the chemical environment of a given element can be obtained using wavelength-dispersive X-ray detection (WDX) and low-energy electron beams generated by field-emission sources in the scanning electron microscope (FESEM). Backscattering detection in the SEM has allowed the detection of polymer domains differentiated by their chemical composition, e.g., polyurethane hard and soft domains, with a few nanometers of resolution,[5] as well as the core−shell morphology in Stöber silica particles[6] and poly(styrene-*co*-acrylamide) latex.[7] The potential of SEM techniques has been largely increased recently with the introduction of commercial focused-ion beam equipment (FIB-SEM).[8]

Other recent microscopy techniques are showing fine details of the distribution of domains characterized by differentiated chemical ambient, even for light elements. This is the case of scanning transmission X-ray microscopy (STXM) and X-ray photoemission electron microscopy (X-PEEM), which are synchrotron-based. Soft X-ray spectromicroscopy techniques provide chemical speciation at better than 50 nm spatial resolution based on near-edge X-ray absorption spectral (NEXAFS) contrast.[9] Methods for converting image sequences to quantitative maps of chemical components were described and illustrated with applications to characterization of wet biofilms, optimization of the synthetic polymer microstructure, and studies of protein interactions with patterned polymer surface. Heat-treated polyacrylonitrile (PAN) fibers were imaged with a spatial resolution of 200 nm by STXM at a third-generation synchrotron radiation facility using NEXAFS spectra to produce chemical state images of the cross-sectioned fiber specimens. A clear "core−rim" structure was observed in the heat-treated fibers.[10] An evaluation of NEXAFS imaging advantages and limitations was recently published.[11] In comparison to electron energy-loss spectroscopy coupled to transmission electron microscopy (TEM-EELS), NEXAFS microscopy has much poorer spatial resolution, but it is more advanta-

* To whom correspondence should be addressed. Phone: +55-19-3521-3080. Fax: +55-19-3521-2906. E-mail: fernagal@iqm.unicamp.br.

(1) Botton, G. Analytical electron microscopy. In *Science of Microscopy*; Hawkes, P. W., Spence, J. C. H., Eds.; Springer: New York, 2007; pp 273−405.
(2) Williams, D. B.; Carter, C. B. *Transmission Electron Microscopy: A Textbook for Materials Science*; Plenum: New York, 1996; Vol. I.
(3) Botton, G. A.; Phaneuf, M. W. *Micron* **1999**, *30*, 109–119.
(4) Egerton, R. F. *Electron Energy-Loss Spectroscopy in the Electron Microscope*; Plenum Press: New York, 1986.
(5) Li, C.; Goodman, S. L.; Albrecht, R. M.; Cooper, S. L. *Macromolecules* **1988**, *21*, 2367–2375.
(6) Costa, C. A. R.; Leite, C. A. P.; de Souza, E. F.; Galembeck, F. *Langmuir* **2001**, *17*, 189–194.
(7) Teixeira-Neto, E.; Leite, C. A. P.; Cardoso, A. H.; da Silva, M. D. V. M.; Braga, M.; Galembeck, F. *J. Colloid Interface Sci.* **2000**, *231*, 182–189.
(8) Stokes, D. J.; Morrissey, F.; Lich, B. H. *J. Phys.: Conf. Ser.* **2006**, *26*, 50–53.
(9) Hitchcock, A. P.; Morin, C.; Zhang, X.; Araki, T.; Dynes, J.; Stoever, H.; Brash, J.; Lawrence, J. R.; Leppard, G. G. *J. Electron Spectrosc. Relat. Phenom.* **2005**, *144−147*, 259–269.
(10) Kikuma, J.; Warwick, T.; Shin, H.-J.; Zhang, J.; Tonner, B. P. *J. Electron Spectrosc. Relat. Phenom.* **1998**, *94*, 271–278.
(11) Hitchcock, A. P.; Dynes, J. J.; Johansson, G.; Wang, J.; Botton, G. *Micron* **2008**, *39*, 311–319.

10.1021/ac8024834 CCC: $40.75
Published on Web 02/17/2009

geous with regard to wet sample analysis. Both techniques are then complementary.

Analytical techniques based on EELS have produced useful information, especially in the case of light elements. This is done in a transmission electron microscope equipped with an electron monochromator yielding energy-filtered (EFTEM)[7,12,13] or electron spectroscopy images (ESI-TEM).[14−17] EELS is based on the inelastic scattering of electrons striking a sample, and the resulting spectra have three main features: zero-loss peak, low-loss region, and the characteristic absorption edges at higher energy, above 100 eV.[18] Absorption edges are useful for elemental analysis since they derive from the inner shell excitation of the sample elements and their large cross sections account for an intrinsically high sensitivity that in turn allows the detection and quantification of very small amounts of any element, even in complex matrixes.

Most ESI-TEM results in the literature are elemental maps, obtained using arithmetic procedures on images acquired above and below the energy threshold for the excitation of inner shell electrons, as for instance the K electrons in C, O, N, and other elements. ESI-TEM elemental maps have been invaluable in elucidating polymer particles and film features so that most of the current microchemical and topochemical information on polymers and polymer composites derives from these maps.[19−22]

The obvious next step in analytical microscopy is molecular mapping, the acquisition of images showing the positions of different molecular constituents within complex systems, either biological or soft materials.

There are two possibilities for molecular mapping that can be implemented using current standard configurations of transmission electron microscopes fitted with EELS spectrometers, but neither has been widely exploited for polymer mapping, as yet.

The first is based on the use of the low-energy-loss spectral features; this means, those derived from inelastic scattering in the 2−80 eV energy range. Another possibility is the use of the spectral fine structure of EELS absorption bands and thus on the same kind of information as NEXAFS, but this will be treated in a separate publication.

The low-energy-loss spectral region has been very useful in the study of semiconductors and metals where it is usually assigned to surface and bulk plasmon losses,[23,24] but it has been much less exploited in the case of dielectric molecular or solid ionic compounds. This is likely due to a single cause: the respective electronic transitions have never received sufficient attention in the literature to create a body of widespread knowledge. However, it is well established that at small scattering angles and high kinetic energies, the most intense transitions are those for which the matrix element of the electric dipole moment is nonvanishing.[25] In the case of rare-earth compounds, where detailed spectroscopic information is available, the low-energy-loss region has been used with success, with an advantage over mapping based on inner shell transitions.[26] By using valence-band states, maps with high spatial resolution yield quantitative elemental composition at high acquisition rates. With the use of Ga 3d and In 4d transitions in the ε_2 absorption spectrum (<40 eV), quantitative elemental maps for III−V device structures were produced for a GaInNAs/GaAs laser structure.

In carbon compounds, the spectral region of low-energy-loss shows some interesting spectral features. In general, inelastic cross sections are large, contributing to high detection sensitivity. In aromatic polymers, a characteristic peak is observed at ~7 eV, which is assigned to an electronic $\pi-\pi^*$ transition.[27,28] This specific feature was applied to the stain-free imaging of polymers[29] differentiating aromatic from aliphatic polymers, in spite of the fact that it is also well established that an aliphatic polymer such as polyethylene can show a $\pi-\pi^*$ spectral feature under electron irradiation, due to hydrogen abstraction followed by reaction between adjacent main-chain carbon atoms.[30] Recent advances in cryoscanning TEM (STEM) associated to EELS were used to quantify the local composition changes, generating distribution maps of water (ice), poly(dimethylsiloxane), and acrylate−vinyl acetate copolymer in individual hybrid particles. The procedure consists in acquiring spectra in different areas of the image, followed by calculation of local composition using multiple least-squares fitting of EELS spectra in the low-loss region.[31,32] A previous work from this laboratory produced two kinds of new results based on low-energy-loss EFTEM imaging. First, images from thick particles and particle aggregates were acquired, where morphological details were obtained even in successively thicker domains by imaging at various energies in the 20−100 eV range.[33] Moreover, mixed particle aggregates imaged in this same range displayed a marked contrast. Contrast intensification, contrast inversion, or blurring was observed at different energies.

(12) Dohi, H.; Horiuchi, S. *Langmuir* **2007**, *23*, 12344–12349.
(13) Valadares, L. F.; Linares, E. M.; Bragança, F. C.; Galembeck, F. *J. Phys. Chem. C* **2008**, *112*, 8534–8544.
(14) Newbury, D. E. *J. Electron Microsc.* **1998**, *47*, 407–418.
(15) Elias, A. L.; Rodriguez-Manzo, J. A.; McCartney, M. R.; Golberg, D.; Zamudio, A.; Baltazar, S. E.; Lopez-Urias, F.; Munoz-Sandoval, E.; Gu, L.; Tang, C. C.; Smith, D. J.; Bando, Y.; Terrones, H.; Terrones, M. *Nano Lett.* **2005**, *5*, 467–472.
(16) Sun, X. H.; Li, C. P.; Wong, W. K.; Wong, N. B.; Lee, C. S.; Lee, S. T.; Teo, B. K. *J. Am. Chem. Soc.* **2002**, *124*, 14464–14471.
(17) Rippel, M. M.; Leite, C. A. P.; Galembeck, F. *Anal. Chem.* **2002**, *74*, 2541–2546.
(18) Goodhew, P. J.; Humphreys, F. J. Chemical analysis in the electron microscope. In *Electron Microscopy and Analysis*, 2nd ed.; Taylor & Francis: New York, 1988; pp 192−198.
(19) Braga, M.; Costa, C. A. R.; Leite, C. A. P.; Galembeck, F. *J. Phys. Chem.* **2001**, *105*, 3005–3011.
(20) Amalvy, J. I.; Percy, M. J.; Armes, S. P.; Leite, C. A. P.; Galembeck, F. *Langmuir* **2005**, *21*, 1175–1179.
(21) Amalvy, J. I.; Asua, J. M.; Leite, C. A. P.; Galembeck, F. *Polymer* **2001**, *42*, 2479–2489.
(22) Valadares, L. F.; Leite, C. A. P.; Galembeck, F. *Polymer* **2006**, *47*, 672–678.
(23) Hagelin, H. A. E.; Weaver, J. F.; Hoflund, G. B.; Salaita, G. N. *J. Electron Spectrosc. Relat. Phenom.* **2002**, *124*, 1–14.
(24) Godinho, V.; Fernández-Ramos, C.; Martínez-Martínez, D.; García-López, J.; Sánchez-López, J. C.; Fernández, A. *Eur. Phys. J.: Appl. Phys.* **2008**, *43*, 333–341.
(25) Lassettre, E. N.; Krasnow, M. E.; Silverman, S. *J. Chem. Phys.* **1964**, *40*, 1242–1258.
(26) Gass, M. H.; Papworth, A. J.; Bullough, T. J.; Chalker, P. R. *Ultramicroscopy* **2004**, *101*, 257–264.
(27) Swanson, N.; Powell, C. J. *Phys. Rev.* **1966**, *145*, 195–208.
(28) Lavilla, R. E.; Mendlowitz, H. *J. Phys. (France)* **1964**, *25*, 114–118.
(29) Arayasantiparb, D.; McKnight, S.; Libera, M. *J. Adhes. Sci. Technol.* **2001**, *15*, 1463–1484.
(30) Ditchfield, R. W.; Grubb, D. T. *Philos. Mag.* **1973**, *27*, 1267–1281.
(31) Kim, G.; Sousa, A.; Meyers, D.; Shope, M.; Libera, M. *J. Am. Chem. Soc.* **2006**, *128*, 6570–6571.
(32) Kim, G.; Sousa, A.; Meyers, D.; Libera, M. *Microsc. Microanal.* **2008**, *14*, 459–468.
(33) Valadares, L. F.; Bragança, F. C.; Silva, C. A.; Leite, C. A. P.; Galembeck, F. *J. Colloid Interface Sci.* **2007**, *309*, 140–148.

There are few examples of detailed studies on electron energy-loss, even for common molecules, and the observed transitions in the low-loss region are not always understood in sufficient detail.[34] One paper concludes that "essentially all the features observed in the discrete excitation region of CH_4, C_2H_6, C_3H_8, and C_4H_{10} can be reasonably assigned to Rydberg transitions by using quantum defects and the transferability of term values",[35] and a recent paper stresses the lack of convergence on the assignments of valence transitions with previous studies. Moreover, most of the Rydberg bands had not been previously assigned even for a simple molecule such as acetic acid, until the observation, analysis, and possible assignments of absorption features between 12 and 20 eV were carried out for the first time in 2006.[36] Nevertheless, by drawing from earlier work on photoelectron spectra of molecules,[37,38] it is possible also to acknowledge contributions to low-energy-loss spectra from first and higher ionization potentials, added to well-known outer shell (L, M) electron excitation.

Concerning the interpretation of images, detailed work by Howie[39] concludes that "spatially valence loss spectroscopy can yield useful and quantitative information about local composition... on the nanoscale provided the geometry of the dielectric interfaces is accurately known." In other cases, the simple assumption of spectrum additive behavior may not always hold.

EFTEM image acquisition in the low-loss spectral region is very interesting, because it requires only low beam exposure, in contrast to currently standard two- or three-windows techniques used for elemental mapping. Moreover, since images are produced by inelastic electrons scattered at low angles, the resolution is nearly as good as in the bright-field images. Thus, the usefulness of the technique depends only on the experimenter's ability to understand the contrast based on known sample chemical, structural, and spectral features.

Thus, this technique holds the potential to produce *molecular maps* within, e.g., polymer blends and nanocomposites, provided that the involved constituents have different low-energy-loss spectra, as shown in this work.

MATERIALS AND METHODS

Latex. Poly(styrene-*co*-hydroxyethyl methacrylate) [P(S−HEMA)] latex was prepared by batch surfactant-free emulsion copolymerization of styrene and 2-hydroxyethyl methacrylate. A detailed description of this reaction is provided in refs 40 and 41. Other samples of styrene−acrylate were commercial resins, Acronal 295 D and Denvercril RA 193, supplied by BASF (São Paulo, Brazil) and Denver (São Paulo, Brazil), respectively.

Nanoparticles. Gold (Ted Pella, $\phi = 4.8 \pm 0.8$ nm), Stöber silica, and aluminum phosphate nanoparticles were used. Silica nanoparticles (33 ± 3 and 143 ± 14 nm diameter, as determined by TEM) were prepared by the method of Stöber et al.[42] Aluminum phosphate pigment is a developmental product[43] supplied by Bunge Company. Effective particle diameter in aqueous dispersion is 332 ± 98 nm, measured using photon correlation spectroscopy (PCS), in a ZetaPlus (Brookhaven Inst. Corp.) at 25 °C.

Particle Submonolayers. Lattices and nanoparticle dispersions were cast and dried forming submonolayers. P(S−BA) and P(S−HEMA) lattices were diluted in water to ca. 0.005% solid content. Gold and Stöber silica nanoparticles ($\phi = 33 \pm 3$ nm) were dispersed in solutions containing poly(*N*-isopropylacrylamide) (PNIPAM) and the surfactant sodium dodecyl sulfate (SDS). The final concentration of polymer and surfactant in the dispersions was 10^{-3} g mL^{-1}, and the particle concentration was 0.006% (in weight). A mixture of styrene−acrylic latex (Denvercril RA 193) and aluminum phosphate was prepared with 20% total pigment volume concentration (PVC). An amount of 76 g of aluminum phosphate slurry was added to 100 g of latex under stirring using a Cowles disperser at 1000 rpm for 1 h. After that, this mixture was diluted in water until a final concentration of 0.006% solid content. A droplet (about 10 μL) of each sample was deposited on carbon-coated parlodion films supported on 400-mesh copper grids (Ted Pella) and allowed to dry at room temperature.

Blend Film Formation. P(S−HEMA) and P(S−BA) lattices were mixed in a proportion of 3:7 w/w at room temperature, stirred for 30 min, and dried in a casting mold at 60 °C.

Ultramicrotomy. Ultrathin (ca. 60 nm) sections for TEM analysis were cut with a diamond knife (Drukker) using a Leica EM FC6 cryoultramicrotome. The blend film was cut at −120 °C, using liquid N_2. A drop of saturated sucrose was used to collect the thin cuts from the cooled microtome and transfer them to the microscope grids. After that, the grids were left floating in deionized water in a beaker for 5−10 min to wash out the sucrose. They were then removed and dried at room temperature.

Stöber colloidal silica ($\phi = 143 \pm 14$ nm) was dried in a glass Petri dish. The dried silica was placed within a silicone rubber mold with 5 mm × 12 mm × 4 mm cavities and embedded in a Pelco Eponate 12 resin (Ted Pella) using the recipe for medium stiffness, followed by curing for 24 h at 60 °C. The embedded silica was cut at room temperature to nominal thickness of 50 nm.

Electron Microscopy. Images were acquired using a Carl Zeiss CEM-902 transmission electron microscope equipped with a Castaing−Henry−Ottensmeyer filter spectrometer. EFTEM was used to obtain high-contrast image series when the slit was set to low-energy-loss and also to obtain bright-field images with low chromatic aberration when the energy slit was selected to zero loss. The series were obtained with an energy slit in the range of 5−20 eV and set to short energy intervals in the 20−100 eV range. ESI-TEM was also used. Characteristic energy losses for C (303 eV) were selected. The images were recorded using a Proscan high-speed slow-scan CCD camera, digitized (1024−1024 pixels, 8 bits) and processed in the iTEM universal TEM imaging platform.

(34) Huang, T.; Hamill, W. H. *J. Phys. Chem.* **1974**, *78*, 2077–2080.
(35) Au, J. W.; Cooper, G.; Burton, G. R.; Olney, T. N.; Brion, C. E. *Chem. Phys.* **1993**, *173*, 209–239.
(36) Leach, S.; Schwell, M.; Un, S.; Jochims, H. W.; Baumgaertel, H. *Chem. Phys.* **2006**, *321*, 159–170.
(37) Dewar, M. J. S.; Worley, S. D. *J. Chem. Phys.* **1969**, *50*, 654–667.
(38) Cooper, G.; Zhang, W.; Brion, C. E.; Tan, K. H. *Chem. Phys.* **1990**, *145*, 117–129.
(39) Howie, A. *Micron* **2003**, *34*, 121–125.
(40) Kamei, S.; Okubo, M.; Matsuda, T.; Matsumoto, T. *Colloid Polym. Sci.* **1986**, *264*, 743–747.
(41) Tamai, H.; Fujii, A.; Suzawa, T. *J. Colloid Interface Sci.* **1987**, *16*, 37–41.
(42) Stöber, W.; Fink, A.; Bohn, E. *J. Colloid Interface Sci.* **1968**, *26*, 62–69.
(43) Galembeck, F.; Brito J. U.S. Patent 20060045831, 2006.

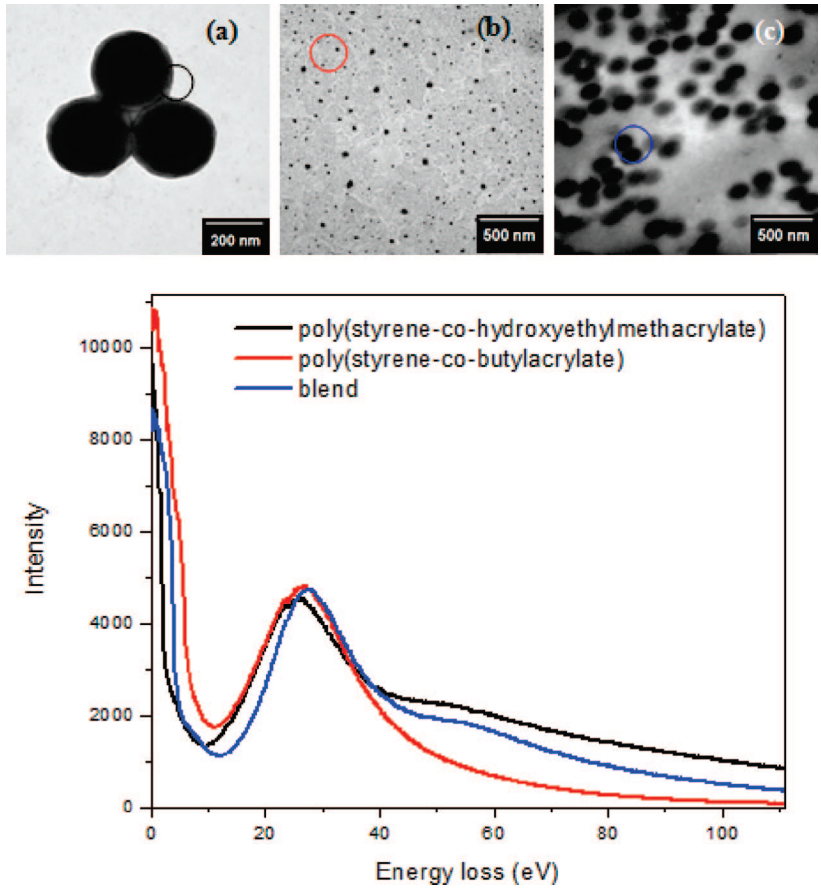

Figure 1. Bright-field images and EEL spectra of (a) poly(styrene−hydroxyethyl methacrylate), (b) poly(styrene−butyl acrylate), and (c) poly(styrene−butyl acrylate)/poly(styrene−hydroxyethyl methacrylate) blend.

RESULTS

The first sample examined is a blend of two styrene−acrylic polymers: P(S−BA) and P(S−HEMA). The first forms flexible plastic films, whereas the second forms brittle colloidal crystals[44] with little or no particle coalescence. Images of the isolated particles supported on the carbon-coated parlodion film are in Figure 1 with the corresponding EEL spectra: both peaks are at ca. 20 eV, but the spectrum from the border of P(S−HEMA) particles also shows another band from 38 to 60 eV, peaking at 48 eV. Beyond, P(S−HEMA) spectrum intensity decreases slower as the energy increases, and it thus is higher from 60 eV up. Figure 1 also shows a bright-field micrograph from a thin blend film cut and its spectrum. It shows the P(S−HEMA) particles dispersed in the P(S−BA) matrix, and the different electron densities of the two polymers produce a pronounced contrast. The spectrum of the blend shows contributions from both components, but these are not additive, which can be expected considering the detailed theoretical work by Howie.

The consequences of the spectral differences are clearly observed in the series of EFTEM images observed in Figure 2, where marked contrast changes are observed in the micrographs obtained at 30, 44, and 60 eV: there is contrast inversion between 30 and 60 eV, and also a thick ring is seen around the particles at 44 eV. This is in agreement with the spectral features shown in Figure 1, and it allows two conclusions: the two different polymers are unequivocally identified and the core−shell structure of the P(S−HEMA) particles is revealed at 44 eV. The sharp contrast changes observed in these images are quite different from the low contrast observed in the K absorption threshold region shown in Figure 3 (280−286 eV) that is normally used for carbon mapping. Indeed, this low contrast is not surprising, considering that this sample is a thin film of a blend of two chemically similar polymers.

Figure 4 shows a set of micrographs and EEL spectra taken from four regions of a sample prepared with aluminum phosphate and styrene−acrylic latex particles. The phosphate aggregates appear very dark in the bright-field image as well as in the 25 eV image, whereas the coalesced latex particles form a gray film in the bright-field micrograph. Above 25 eV, small morphological details can be observed within thick domains that are completely dark in the bright-field as well as in the 25 eV image. All EEL spectra are dominated by single peaks within the 20−30 eV range, which are all very similar but with some qualitative differences. Spectral intensities of areas containing aluminum phosphate decrease as the energy increases slower than the polymer spectrum. Spectra from regions containing aluminum phosphate and polymer domains cross at ca. 40 eV. This means that aluminum phosphate domains become increasingly brighter in the 45−105 eV loss images. This observation is stressed in the 25 and 85 eV overlay images, where the aluminum phosphate aggregates and the polymer domains appear orange and blue, respectively. Furthermore, this superimposed image shows clearly the polymer surrounding phosphate aggregates.

(44) Galembeck, A.; Costa, C. A. R.; Silva, M. C. V. M.; Galembeck, F. *J. Colloid Interface Sci.* **2001**, *234*, 393–399.

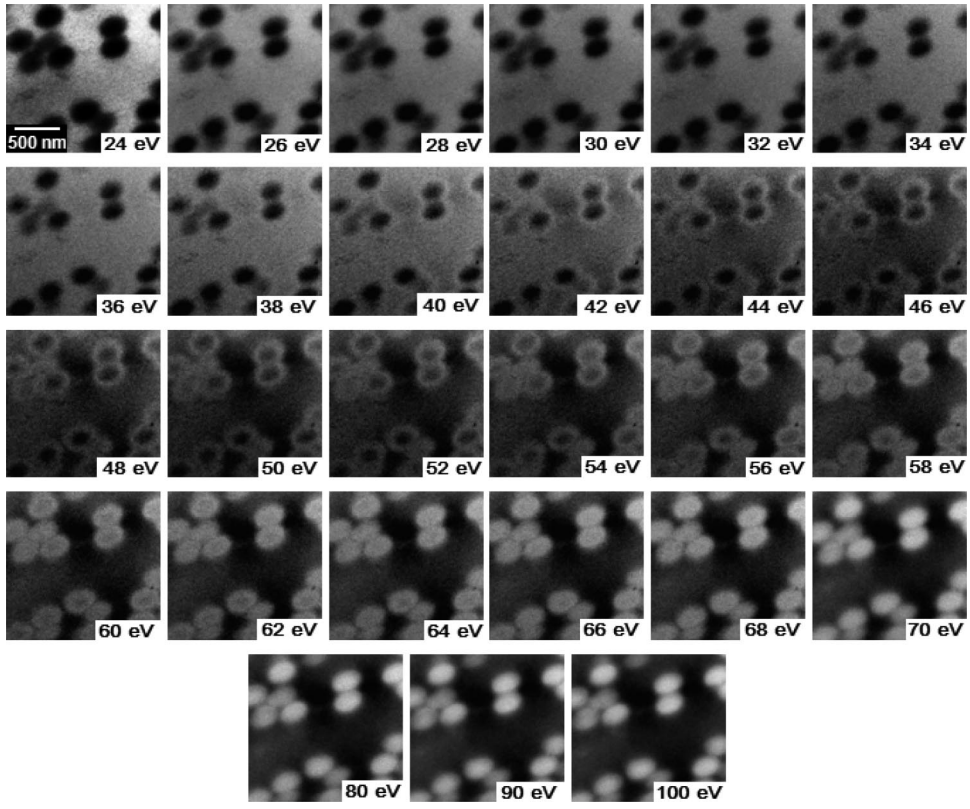

Figure 2. Low-loss EFTEM images (24−100 eV energy loss) of a thin cut from a blend of poly(styrene-*co*-hydroxyethylmethacrylate) with poly(styrene−butyl acrylate).

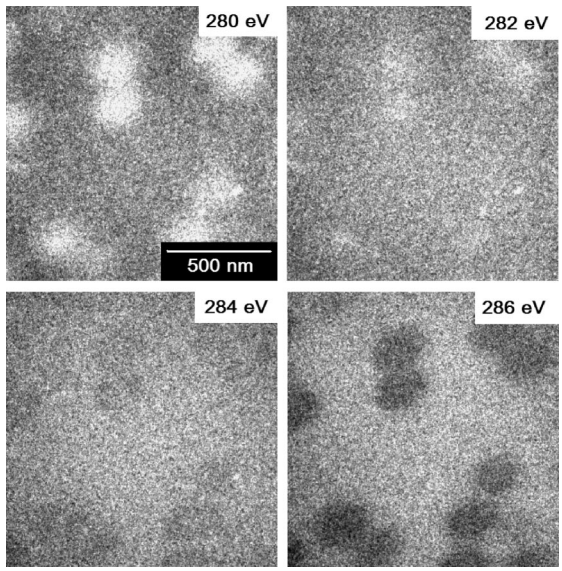

Figure 3. EFTEM images (280−286 eV energy loss) of a thin cut from a blend of poly(styrene-*co*-hydroxyethylmethacrylate) with poly(styrene−butyl acrylate).

In Figure 5, a bright-field image and a series of EFTEM images of a submonolayer of Stöber silica nanoparticles are shown. Before drying on the TEM sample holder grid, the particles were dispersed in an aqueous solution of polymer (PNIPAM) and surfactant (SDS) that adsorb at the nanoparticles surface.[45,46] The bright-field image shows small groups of nanoparticles, seemingly separated, whereas the image at 25 eV shows particles apparently larger and contoured by a brighter ring (in the color pictures, darker colors mean brighter areas), revealing the presence of the adsorbed constituents. As the energy increases in the range from 25 to 50 eV, the images change gradually losing contrast between particle inner and outer regions. This effect is clearly seen in Figure 5 overlaying images at 25 and 50 eV.

Images of gold nanoparticles dispersed in the same polymer−surfactant solution are presented in Figure 6. The bright-field image shows an area with many individual particles, but again, the images at lower energy (25 and 30 eV) reveal that particle interstices are filled with adsorbed material, together with some structured material deposited on the sample background. At 40 and 50 eV, the particle interior is highlighted. Contrast inversion is observed at 25 eV and also overlaying images at 25 and 50 eV. For the sake of comparison, a carbon map is also presented, but it does not show the fine detail observed in the low-loss images.

Figure 7 gives a set of bright-field and low-loss EFTEM images taken from thin cuts of Stöber silica embedded in resin. The EFTEM images in the 25−65 eV range show differentiated contrast on the central region of some sliced silica particles, showing that particles are inhomogeneous. The core-and-shell nature of these particles is also clearly shown with good resolution, confirming results obtained in a previous work from this laboratory.[47]

An advantage of the low-loss images is that particles are not deformed during image acquisition, and the bright-field images taken before and after mapping are identical. However, the same

(45) Rezende, C. A.; Lee, L. T.; Galembeck, F. *Langmuir* **2008**, *24*, 7346–7353.
(46) Costa, C. A. R.; Leite, C. A. P.; Lee, L. T.; Galembeck, F. *Prog. Colloid Polym. Sci.* **2004**, *128*, 74–80.
(47) Costa, C. A. R.; Leite, C. A. P.; Galembeck, F. *J. Phys. Chem. B* **2003**, *107*, 4747–4755.

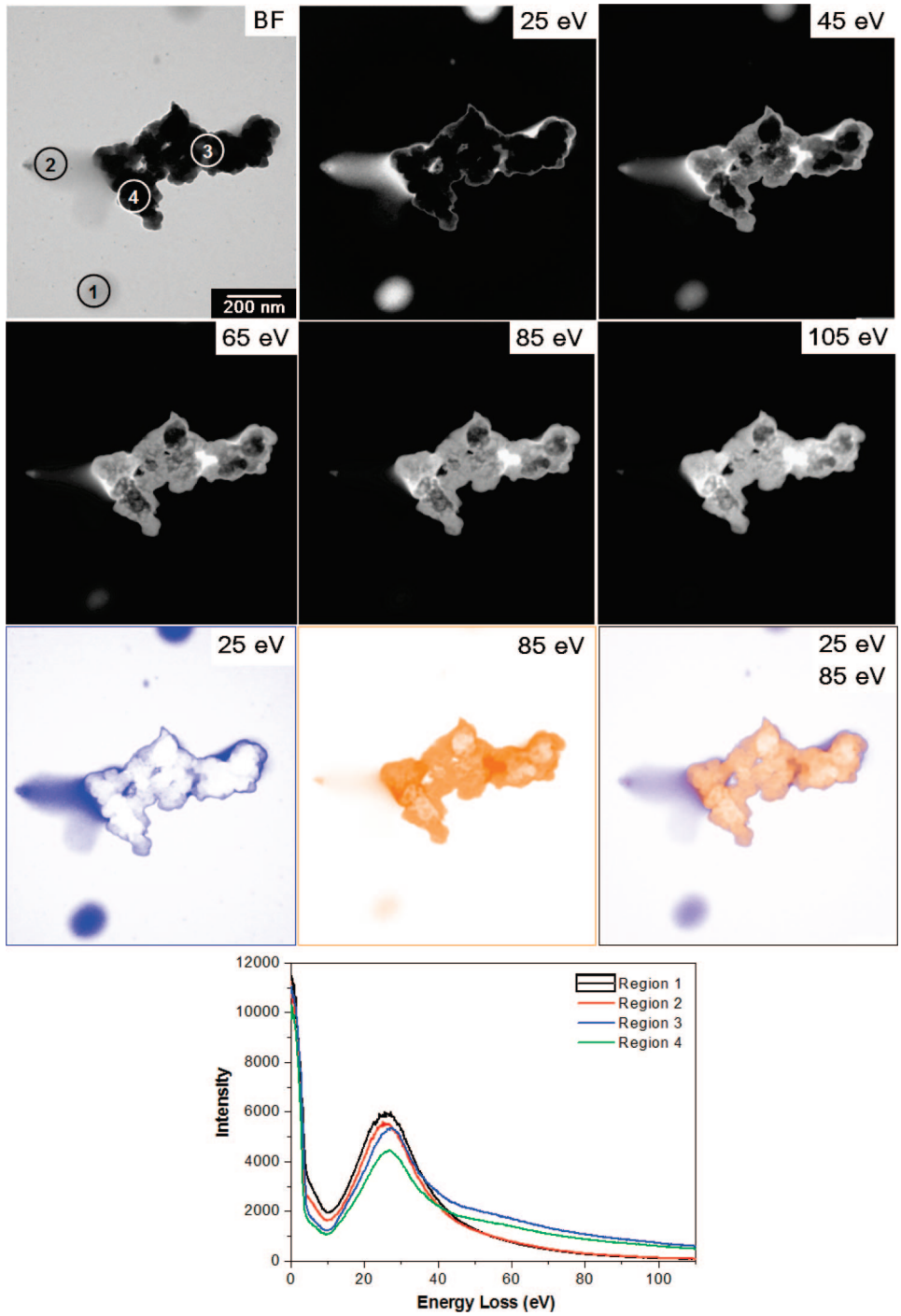

Figure 4. (a) Bright-field, series of EFTEM, and pseudocolor EFTEM images (25 and 85 eV) from a submonolayer prepared by drying a dispersion of poly(styrene−butyl acrylate) and aluminum phosphate. (b) EEL spectra of four different regions indicated in the bright-field image.

particles undergo detectable deformation when images are acquired at higher energy loss, due to the use of a more intense beam.

DISCUSSION

In ordered systems, electron microscopy imaging of heavier elements within molecules has now reached the atomic resolution limit,[48] and molecular resolution has been achieved by using scanning tunneling microscopy (STM),[49] but it is unclear if those approaches will allow the examination of organic molecules in less-ordered supramolecular arrays. This is especially important in the case of macromolecules, either in nanostructured materials or in biological systems.

Following the approach described in this paper, domains with different molecular compositions are distinguished in low-energy-loss images, with nanometer resolution, thanks to minute but

(48) Haruta, M.; Yoshida, K.; Kurata, H.; Isoda, S. *Ultramicroscopy* **2008**, *108*, 545–551.

(49) Nion, A.; Jiang, P.; Popoff, A.; Fichou, D. *J. Am. Chem. Soc.* **2007**, *129*, 2450–2451.

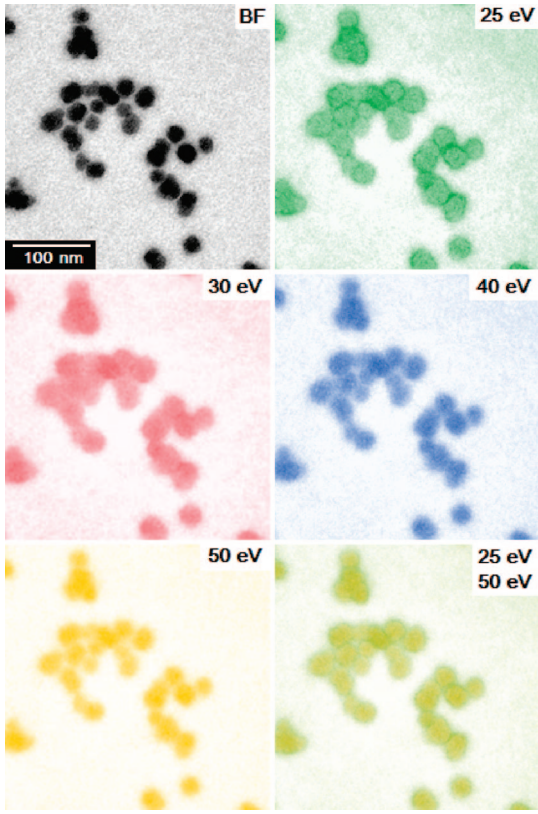

Figure 5. Bright-field and a series of EFTEM images from a submonolayer of Stöber silica nanoparticles dispersed in PNIPAM and SDS and dried at room temperature. The last shot on the right results from the overlay of the images at 25 (green) and 50 eV (yellow).

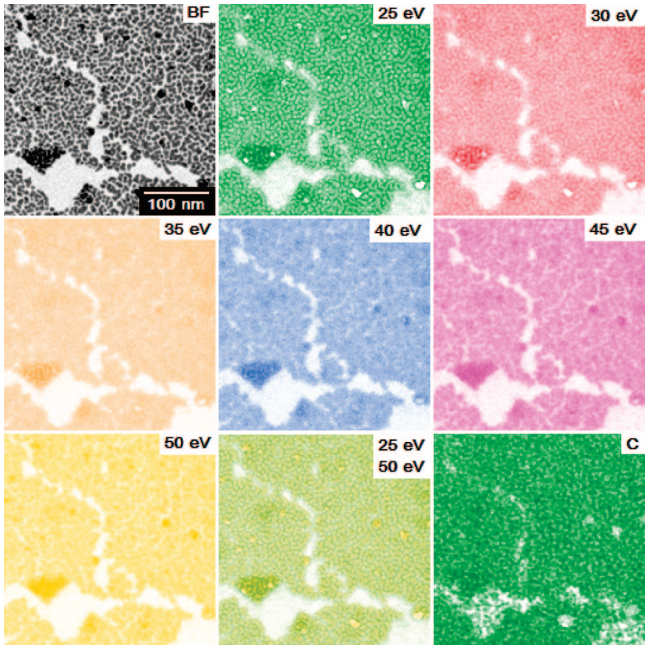

Figure 6. Bright-field and a series of EFTEM images from a submonolayer of gold nanoparticles dispersed in PNIPAM and SDS and dried at room temperature. In the last shot there is a carbon map of the same field.

decisive differences in the respective electronic spectra that derive from the overall electronic structure.

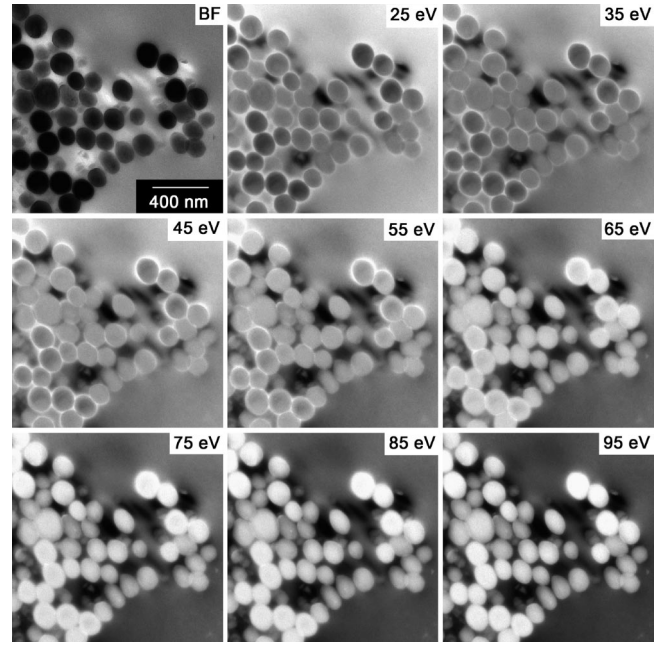

Figure 7. (Top left) Bright-field image and low-loss EFTEM images (25−95 eV energy loss) of embedded Stöber silica thin cuts.

Thus, the present approach offers significant advantages in noncrystalline systems, especially in the case of macromolecular compounds, where the researcher cannot count on the use of geometric parameters related to well-defined molecular dimensions to gain information, as is often done in molecular imaging by atomic force microscopy (AFM) or STM. These advantages are shared with the photoemission methods, but these currently have lower spatial resolution than EFTEM or ESI-TEM.

The availability of EEL spectra in the 1−100 eV region is useful but not essential for differentiating domains in the low-energy-loss region. In Figures 4−7, spectra are not shown for the systems, but it is still possible to interpret the images unequivocally, provided at least one material presents a well-defined geometry.

An excellent contrast is observed within different domains, even though the low-energy-loss spectra for molecular solids have few sharp features. Moreover, not only contrast is obtained at a given energy-loss but also the contrast patterns change with the imaging electron energy, producing a large amount of detailed information irrespective of the sample complexity. Thus, this technique is especially suitable for discovering differentiated molecular domains in a complex sample.

The series of EFTEM images of P(S−HEMA)/P(S−BA) blend film shows the sensitivity of this technique to contrast materials with similar chemical compositions. Both materials are copolymers of styrene and acrylate monomers, and they produce low contrast in the K threshold region. However, using low-energy-loss EFTEM each polymer phase is easily observed as well as the P(S−HEMA) core−shell structure. Core−shell composition difference is also revealed in the images of ultramicrotomed Stöber silica particles. In the case of polymer layers adsorbed on the surface of gold and silica nanoparticles, the contrast between the inner and the outer regions of the particles in EFTEM images change gradually as the energy increases from 25 and 50 eV, providing clear identification of the adsorbed material, with good spatial resolution.

Images with contrast due to differences in the molecular composition at nanometer resolution are thus obtained. This can be done even in cases where little or no previous information is available on the sample constituents. The achieved resolution matches the excellent results that have been obtained by AFM[50] but with an advantage in the case of systems that are in an early stage of investigation.

The expression "molecular mapping" was previously used, but the involved techniques employed other approaches that suffer from various limitations and found only a rather limited use.[51,52] Given the characteristics of the present technique, it can well find widespread application.

In conclusion, there is no barrier to finding out the distribution of different molecular constituents in a sample, with at least nanometer resolution. Achieving atomic resolution will largely depend on the experimenter's ability to image soft materials with high-energy beams, without introducing excessive sample damage. This is not a simple task, but it is certainly worthwhile, for those interested in learning about the structural arrays existing in natural or synthetic complex materials to understand their properties and possible functions.

(50) Kienberger, F.; Ebner, A.; Gruber, H. J.; Hinterdorfer, P. *Acc. Chem. Res.* **2006**, *39*, 29–36.

(51) Martin, J. M.; Vacher, B.; Ponsonnet, L.; Dupuis, V. *Ultramicroscopy* **1996**, *65*, 229–238.

(52) Diociaiuti, M.; Falchi, M.; Paoletti, L. *Microsc., Microanal., Microstruct.* **1995**, *6*, 33–40.

CONCLUSIONS

EFTEM serial imaging in the low-energy-loss spectral region allows the observation and distinction of domains with sizes in the nanometer range and with small differences in chemical composition, without staining the sample. This is done under low sample exposure to the electron beam without introducing detectable sample damage even in very soft materials, producing accurate molecular distribution maps.

ACKNOWLEDGMENT

E.M.L., C.A.R., C.A.S., and L.F.V. express thanks for fellowships from Fapesp, CAPES, and CNPq. This is a contribution from the Millennium Institute for Complex Materials, PADCT/CNPq. F.G. acknowledges useful discussions with Professors Oscar Malta (Recife) and Gerardo G. B. de Souza (Rio de Janeiro).

SUPPORTING INFORMATION AVAILABLE

(S1) Description of two sample preparation procedures (a) poly(styrene-*co*-hydroxyethyl methacrylate) [P(S−HEMA)] latex and (b) Stöber silica, and (S2) a full set of pictures from which Figure 2 was extracted. This material is available free of charge via the Internet at http://pubs.acs.org.

Received for review November 24, 2008. Accepted January 15, 2009.

AC8024834